Malaysian Journal of Civil Engineering 26(2):224-250 (2014)

NONLINEAR ANALYSIS OF CONCRETE DEEP BEAM REINFORCED WITH GFRP BARS USING FINITE ELEMENT METHOD

Ibrahim M. Metwally*

Concrete Structures Reasearch Institute, Housing & Building Research Centre, P.O. Box 1770 Cairo, Egypt

*Corresponding Author: *dr_ibrahimmetwally@yahoo.com*

Abstract: The efficient use of FRP reinforcement in deep members has been hindered due to a lack of knowledge on the behavior of such members. Till now, most of researches have mainly focused on the flexural or shear behavior of shallow members longitudinally reinforced with FRP and most of them testing at small scales. This paper presents numerical investigation of twelve large-scale concrete deep beams internally reinforced with GFRP bars without web reinforcement failed in shear which were experimentally tested and collected from literature. The collected specimens cover several parameters which usually influenced on strength and behavior of deep beams as shear span / depth ratio, the reinforcement ratio, the effective depth, and the concrete strength. Concrete deep beams are generally analyzed using conventional methods such as empirical equations or strut and tie models. These methods however do not take into account the redistribution of forces resulting from non-linear materials' behaviors. To address this issue, non-linear finite element analysis that incorporates non-linear material behavior as ABAQUS package will be used. It was found completely efficient in handling such analysis and the proposed simulation of the material in the present study are capable of predicting the real behavior of reinforced concrete deep beam reinforced with GFRP bars in terms of load-deflection behavior, failure load, failure mode, crack propagation, GFRP reinforcement strain, and concrete strain distribution similar to the tested large scale deep beams. Besides, deep beam reinforced with GFRP bars showed different behavior than that of beam reinforced with CFRP bars due to the low elastic modulus of GFRP bars, which was increased dramatically the deflection. Thus, the deflection, instead of strength will govern the design for concrete deep beam reinforced with FRP bars.

Keywords: *Deep beam; GFRP bars; finite element; ABAQUS*

1.0 Introduction

Corrosion of steel reinforcement in concrete structures leads to cracking and spalling of concrete, resulting in costly maintenance and repair. An innovative solution to such a problem can be provided by using fiber-reinforced polymer (FRP) as an alternative to steel reinforcement. FRPs are corrosion-free materials and have recently shown a great

potential for use in structural applications because of their high strength-to-weight ratio. Therefore, replacing the steel reinforcement with the non-corrosive FRP reinforcement eliminates the potential of corrosion and the associated deterioration.

Extensive research programs have been conducted to investigate the flexural and shear behavior of slender (shallow) concrete members reinforced with FRP reinforcement(Andermatt and Lubell, 2013A). Very little experimental data and nearly no finite element analysis exist for FRP-reinforced concrete deep beams. So, shear behavior of them has not been sufficiently understood.

The shear capacity of deep beams is a major issue in their design. The behavior of reinforced concrete deep beams is different from that of slender beams because of their relatively larger magnitude of shearing and normal stresses. Unlike slender beams, deep beams transfer shear forces to supports through compressive stresses rather than shear stresses. There are two kinds of cracks that typically develop in deep beams: flexural cracks and diagonal cracks. Diagonal cracks eliminate the inclined principal tensile stresses required for beam action and lead to a redistribution of internal stresses so that the beam acts as a tied arch. The arch action is a function of a/d(shear span/ depth) and the concrete compressive strength, in additional to the properties of the longitudinal reinforcement. It is expected that the arch action in FRP reinforced concrete would be as significant as that in steel reinforced concrete and that the shear strength of FRP-reinforced concrete beams having a/d less than 2.5 would be higher than that of beams having a/d of more than 2.5 (Nawy, 2003).

The application of the reinforced concrete deep beams within structural engineering practice has risen substantially over the last few decades. More specially, there has been an increased practice of including deep beams in the design of tall buildings, offshore structures, wall tanks and foundations. They differ from shallow beams in that they have a relatively larger depth compared to the span length. As a result the strain distribution across the depth is non-linear and cannot be described in terms of uni-axial stress strain characteristics (Islam and Khennane, 2012). Prediction of behavior of deep beams by design codes which contains empirical equations derived from experimental tests have some limitations. They are only suitable for the tests conditions they were derived from, and most importantly, they fail to provide information on serviceability requirements such as structural deformations and cracking. Likewise, the strut and tie model, although based on equilibrium solutions thus providing a safe design, does not take into account the non-linear material behavior and hence also fails to provide information on serviceability requirements. Cracking of concrete and yielding of steel are essential features of the behavior of concrete structures and, therefore, they must be taken into account in predicting their ultimate load capacity as well as service behavior. Failure to do so simply means that the redistribution of stresses in the structure is not taken into account (Enem *et al*., 2012). Thus, the development of an alternative analysis method by FE is needed to understand its behavior. As reported by Enem *et al*., (2012), that

finite element method (FEM) offers a powerful and general analytical tool for studying the behavior of reinforced concrete deep beams. Finite element method as a tool can provide realistic and satisfactory solutions for linear and nonlinear behavior of deep beam structural elements. Accordingly, it is very needed to generate reliable FE models that can be utilized to enhance the understanding of the fundamental structural response of the FRP-reinforced deep beams and hence optimize its design.

The main objective of this study is to investigate capabilities of the finite element simulation for further study on GFRP-reinforced concrete deep beam behavior instead of conducting expensive time consuming experimental works of large-scale structural elements.

2.0 Experimental Technique

2.1 Characteristics of Tested Deep Beams

Twelve concrete deep beams internally reinforced with GFRP bras were collected from literature (Andermatt and Lubell, 2013A). They were constructed and tested to failure. The primary test variables included the a/d, the reinforcement ratio ρ, the effective depth d, and the concrete strength f_c'. The objective of the test program was to assess the design parameters that influence the strength and behavior of FRP-reinforced concrete deep beams without web reinforcement. The configuration of the specimens is given in Table 1 and Figure1. The a/d of the specimens were selected to cover a wide range of the deep beam category at the ultimate and equivalent serviceability limit states and to fill gaps in the limited experimental data available on FRP-reinforced concrete deep beams. Specimens were grouped into three series having nominal heights h of 300, 600, and 1000 mm. To study the effect of concrete strength on the shear capacity, both normal- and high-strength concretes were used. The reinforcement in all specimens consisted of GFRP bars, as this is the most commonly used FRP in the industry. The reinforcement ratios were selected such that the stress level in the FRP would not exceed approximately 25% of the specified tensile strength (f_{FRPu}) of the GFRP bar under the equivalent serviceability limit state loads(Andermatt and Lubell, 2013A). Note that ACI Committee 440(2006) limits the service stress level in the GFRP to 0.20 f_{FRPu}. Overhang lengths were provided beyond the supports in all specimens to allow for anchorage of the FRP reinforcement(Andermatt and Lubell, 2013A).

Table 1: Characteristics of GFRP-Reinforced Concrete Deep Beams (Andermatt and Lubell, 2013A)

Specimen	ρ, %	Height (h), mm	Width (b_w), mm	Shear span (a), mm	a/d	Overhang length, mm*	f_c', MPa
A1N	1.49	306	310	276	1.07	874	40.2
A2N	1.47	310	310	376	1.44	874	45.4
A3N	1.47	310	310	527	2.02	874	41.3
A4H	1.47	310	310	527	2.02	623	64.6
B1N	1.70	608	300	545	1.08	605	40.5
B2N	1.71	606	300	743	1.48	605	39.9
B3N	1.71	607	300	1040	2.07	605	41.2
B4N	2.13	606	300	736	1.48	814	40.7
B5H	2.12	607	300	736	1.48	614	66.4
B6H	1.70	610	300	1040	2.06	460	68.5
C1N	1.58	1003	301	974	1.10	826	51.6
C2N	1.56	1005	304	1329	1.49	821	50.7

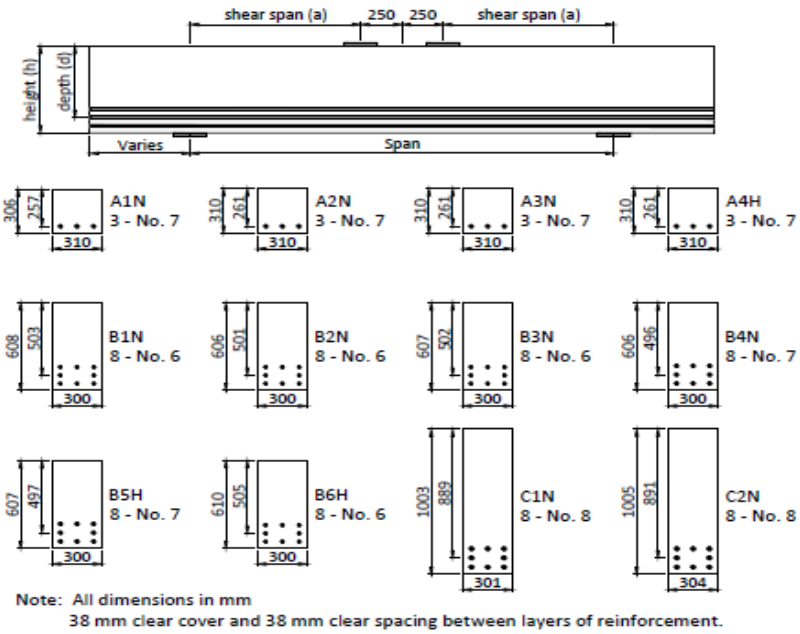

Figure 1: Test Setup and Specimen Geometry(Andermatt and Lubell, 2013A)

2.2 Testing Setup

Deep beams were tested in a 6600 kN capacity testing frame under four-point loading as a simple beam. Five linear variable differential transformers (LVDTs) were mounted along the bottom of the specimens to measure vertical deflection at the supports, quarter-spans, and mid-span. Electrical resistance strain gauges were applied to the FRP bars to measure the strain during the test. Each specimen was loaded in five to 10 increments. After each increment, the deflection was held while the crack patterns were photographed. Data from the instrumentation were recorded continuously until specimen failure(Andermatt and Lubell, 2013A).

3.0 Finite Element Study

The general purpose FE software ABAQUS (ABAQUS,2014) was employed to generate FE models to simulate numerically the structural response of the previously described concrete deep beams reinforced with GFRP bars. The generated models were validated against all respective experimental results.

3.1 Constitutive Models

3.1.1 Concrete Model

The damaged plasticity model for concrete available in the ABAQUS material library was adopted to model concrete response, since it has been shown to perform satisfactorily in similar applications (Malm, 2009). This model is used for concrete plastic behavior. It is very versatile and capable of predicting the behavior of concrete structures subjected to monotonic, cyclic and dynamic loading. It assumes that the two main failure mechanisms in concrete are the tensile cracking and the compressive crushing. In this model, the uni-axial tensile and compressive behavior is characterized by damaged plasticity(ABAQUS,2014). Required parameters for defining the plastic properties of concrete are: *ψ(dilation angle), ε(flow potential eccentricity), fb/fc(ratio of biaxial compressive ultimate strength/ uniaxial ultimate compressive strength), k(ratio of tension meridian plane to the second stress invariant of compression meridian plane), and μ(viscosity parameter)* , were assumed 15°, 0.1, 1.16, 0.667, and 0.026 respectively. The mechanical properties of the used concrete were measured experimentally for all specimens under both compression and tension as shown in Table 2.

Table 2 : Experimentally Measured Concrete Properties(Andermatt and Lubell, 2013A)

Beam Code	Ultimate Compressive Strength , *MPa*	Young's Modulus, *MPa*	Strain at ultimate strength	Strain at end of softening curve	Ultimate Tensile Strength, *MPa*	Poisson's Ratio
A1N	40.2	23020	0.0027	0.0039	2.10	0.2
A2N	45.4	22850	0.0028	0.0040	2.22	0.2
A3N	41.3	24150	0.0026	0.0040	2.12	0.2
A4H	64.6	22450	0.0032	0.0040	2.65	0.2
B1N	40.5	23320	0.0024	0.0038	2.10	0.2
B2N	39.9	23210	0.0025	0.0031	2.08	0.2
B3N	41.2	23680	0.0027	0.0030	2.12	0.2
B4N	40.7	24290	0.0025	0.003096	2.10	0.2
B5H	66.4	24140	0.0034	0.0042	2.70	0.2
B6H	68.5	24010	0.0033	0.0036	2.73	0.2
C1N	51.6	26870	0.0026	0.0040	2.37	0.2
C2N	50.7	25260	0.0027	0.0040	2.35	0.2

3.1.2 GFRP reinforcement

GFRP rebars were simulated as elastic isotropic one dimensional material until failure, as recommended by Al-Musallam *et al*. (2013). Using one tensile modulus of elasticity, one Poisson's ratio and one shear modulus. This is because shear deformation in the bar itself is so small to ignore . The test results of GFRP bars are tabulated in Table 3.

Table 3 : Experimental Tension Test Results of the Used GFRP Bars(Andermatt and Lubell, 2013A)

Bar No.	Bar Diameter, mm	Area, mm^2	Failure Stress, (f_{fu}), MPa	Modulus of Elasticity, (E_f), MPa	Rupture strain, %	Poisson's Ratio (υ)
# 6	19	322	765	37900	1.8	0.26
# 7	22	396	709	41100	1.7	0.26
# 8	25	528	938	42300	2	0.26

3.2 Elements

The ABAQUS element library provides a complete geometric modeling capability. For this reason any combination of elements can be used to make up the model. All elements use numerical integration to allow complete generality in material behavior. Element

properties can be defined as general section behaviors, or each cross -section of the element can be integrated numerically, so that nonlinear response can be tracked accurately when needed.

3.2.1 Solid Element

The solid (or continuum) elements in ABAQUS can be used for linear analysis and for complex nonlinear analyses involving contact, plasticity, and large deformations. Regarding the finite element models introduced in this work, three dimensional 8-node first order fully integration continuum elements (C3D8 - Bricks) are used to model the concrete deep beams and loading and bearing plates.

3.2.2 Truss Element

The other basic components in this study are the reinforcing bars for longitudinal reinforcement. The reinforcing bars have mainly the task to transfer normal forces. For that purpose, reinforcing bars are modeled as three -dimensional truss elements are sufficient for the purpose. Three dimensional 2-node first order truss elements (T3D2 - Truss) are used to model the GFRP reinforcing bars in the FE model of concrete beam specimens.

3.3 Meshing

In order to obtain accurate results from the FE model, all the elements in the model were purposely assigned the same mesh size to ensure that each two different materials share the same node. The type of mesh selected in the model is hexahedron (brick) structured element. The mesh element for modeling of concrete and steel loading and bearing plates is 8-node brick elements with three translation degrees of freedom at each node (C3D8) . Discrete GFRP rebar can be defined only by truss element which is called T3D2(3Dimensional-2Node truss element). Figure 2(a) shows the typical mesh of the FE model of deep beam specimens. Modeling and mesh generation is developed using same techniques for all specimens. To verify the FE analysis and mesh sensitivity, five different mesh sizes were selected for the simulation of the deep beams (150, 125, 100, 75, and 50 mm). The load-deflection curves obtained from FE model at different mesh size for C2N beam were compared with the experimental one. The FE models with the different mesh sizes were found to represent the behavior of GFRP- reinforced concrete deep beams well as shown in Figure 2(b). Mesh density 100 ×100 ×100 mm attained higher accuracy (among the other mesh densities)with respect to the ultimate load capacity and the corresponding central deflection compared to the experimental results. So, it has been adopted in the finite element analyses in this research work.

3.4 Boundary Conditions and Loading

The boundary conditions for the models created with 3D solid elements representing the supporting plates are defined as follows:

Pin Support: The nodes along the transverse line at the middle bottom of the supporting plate were locked against translation in all directions vertical (y-direction), transverse (x-direction) and longitudinal (z-direction). These nodes are free to rotate about all axes.

Roller support: The nodes along the transverse line at the middle bottom of the supporting plate were locked against translation in only one vertical direction (y-direction). These nodes are free to rotate about all axes. The loading profile is applied to the model. The loading plate serves as a medium that uniformly distributes the pressure on the loaded area. For finite element model loading, and defined boundary conditions can be seen in Figure 2(c).

3.5 Interactions

ABAQUS provides many different facilities for modeling the interactions between model parts. These facilities enable model approaching to accurately simulate the experimental behavior of the tested beam specimens that was observed from the experimental program.

3.5.1 Interaction Between GFRP bars and Surrounding Concrete

Andermatt and Lubell (2013A) reported in their experimental work that the used GFRP bars were coated with sand layer which achieved a higher bond. Consequently, full bond(perfect bond) was considered between GFRP bars and surrounding concrete in the FE model. In this study, truss elements are used to represent the GFRP reinforcement bars, and these are embedded in "host" continuum solid elements(concrete). Embedding means that the translational degrees of freedom at the nodes of the embedded element are eliminated and become constrained to the corresponding interpolated values in the host continuum element. The solid parts with embedded reinforcement approach assumes perfect bond only at the embedded nodes. Hence, if the embedded element has nodes at the edges of the host element only, then the reinforcement becomes free within the host element. If multiple embedded nodes are used with the host element, then perfect bond is assumed at these nodes.

3.5.2 Interaction Between Deep Beam and loading and bearing Steel Plates

Both loading and bearing plates are connected to beam specimen using tied contact (is available in ABAQUS constraint module) was used with no separation interaction

behavior between the concrete surface and plates which means that parts cannot be disconnected during loading.

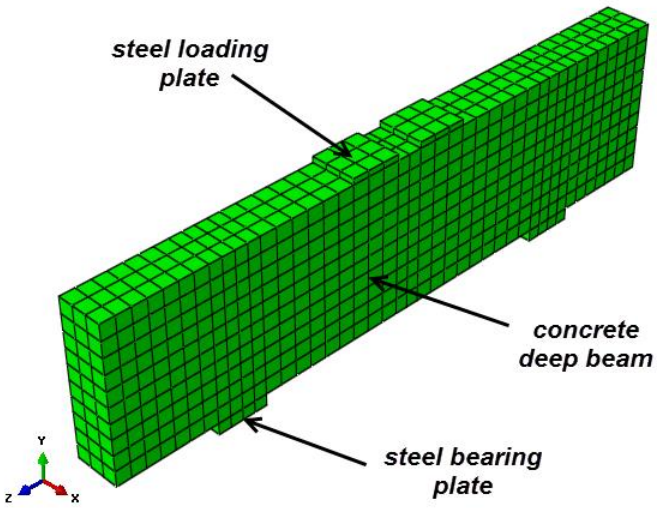

Figure 2(a)- 3-D Meshing of Concrete Deep Beam Model in ABAQUS

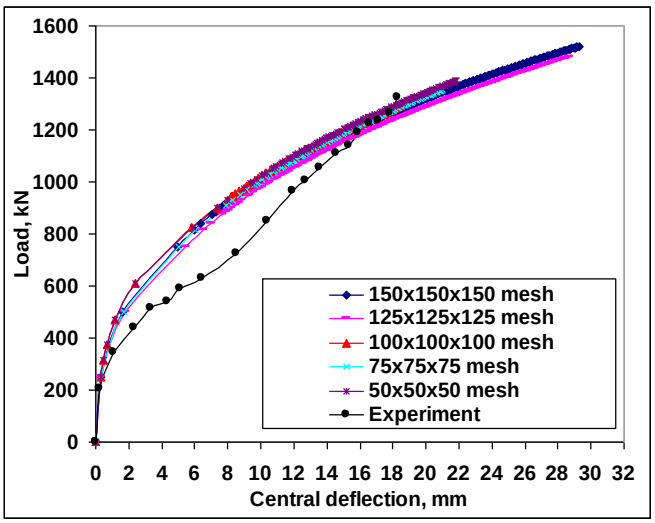

Figure 2(b)- Comparison of Load-Deflection Curves of FEM with Different Mesh Sizes and Experimental Result of Beam C2N

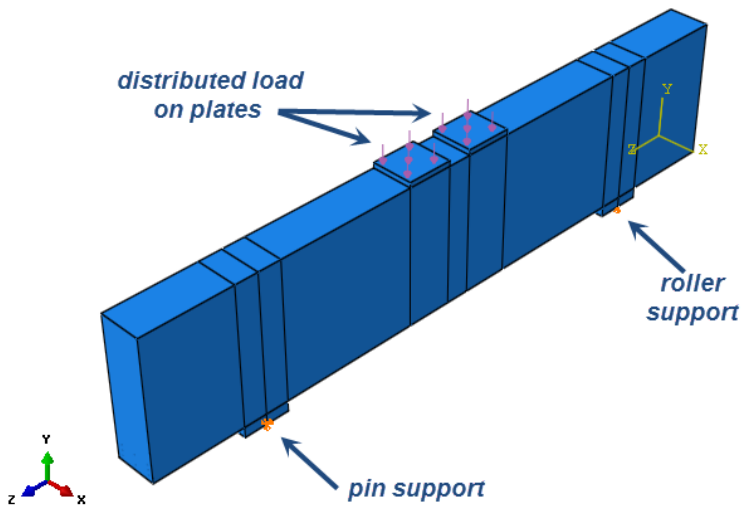

Figure 2(c)- Loading Profile and Boundary Conditions

4.0 Numerical Analysis :Verification of FE Model

4.1 Load-Deflection Responses

To verify the proposed FE model, a comparison of load–midspan deflection response acquired from test results is demonstrated. The comparison between experimental and the numerical load-deflection curves for the mid span deflection of the deep beams reinforced with GFRP bars are shown in Figure 3. It shows that the finite element load deflection curves are somewhat stiffer than the experimental plots. After first cracking, the stiffness of the finite element models is again higher than that of the experimental beams. There are several effects that may cause the higher stiffness in the finite element models. The most important is microcracks which are present in the concrete for the experimental deep beams, and could be produced by drying shrinkage in the concrete and/or handling of the deep beams. On the other hand, the finite element models do not include the microcracks. As well known that the microcracks reduce the stiffness of the experimental deep beams. For all specimens, good agreement is in load-deflection relation prior to failure load. For each of the test deep beams, the predicted and the measured maximum loads and deflections were in good agreement. The values given by all specimens were similar to the analytical results; comparative data are summarized in Table 4. The mean ratios of experimental-to-numerical ultimate load (predicted by ABAQUS) were 1.01 at a standard deviation of 0.05. Also, finite element analysis gives

an accurate values of mid-span deflection for deep beams , the average ratios of experimental to predicted deflection at ultimate load equal 0.98 with standard deviation equal 0.07. In general, the load-deflection curve from the experiment and the FEM analysis were in very good agreement. This indicates that the constitutive models used for concrete and GFRP bars able to capture the fracture behavior of GFRP-reinforced deep beam accurately.

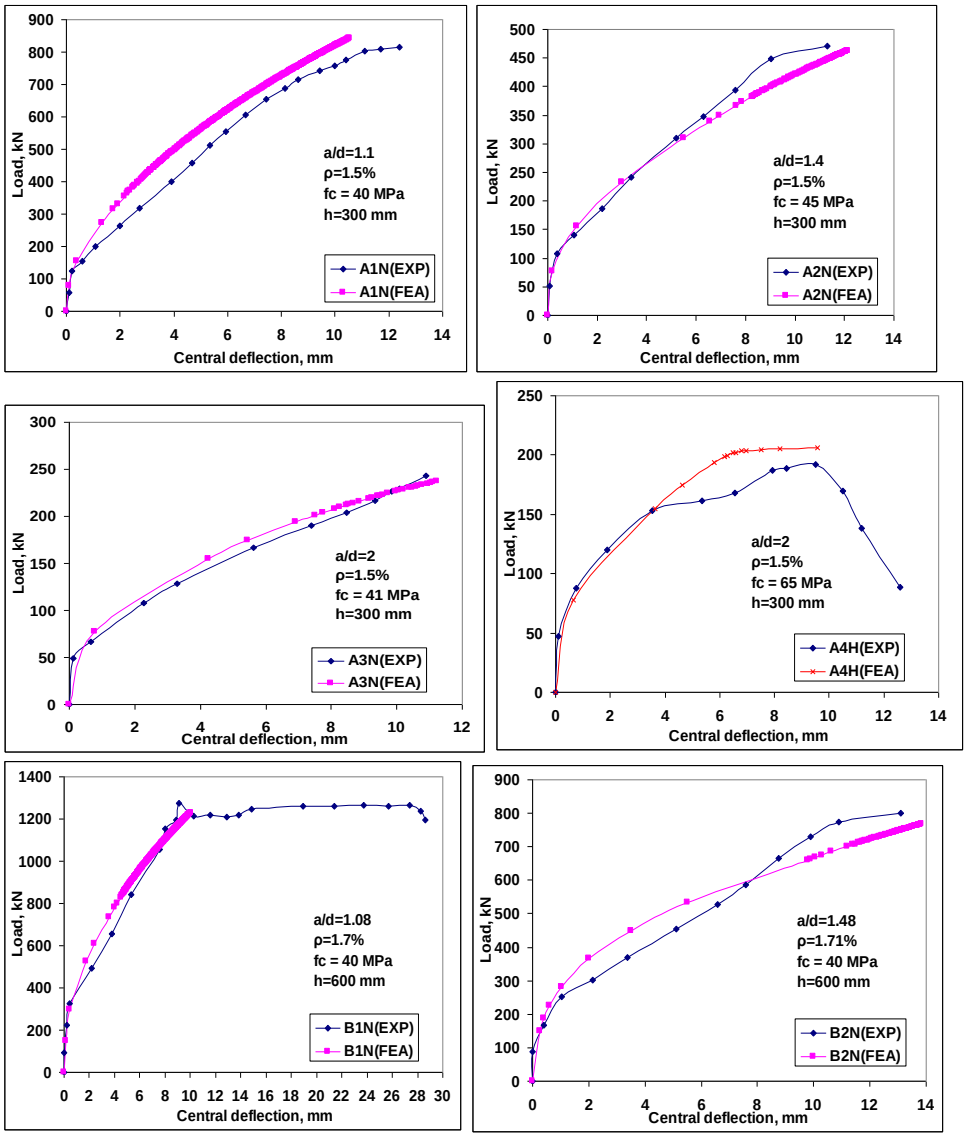

Figure 3: FE Versus Experimental Load-Deflection Curves of the Studied Deep Beams

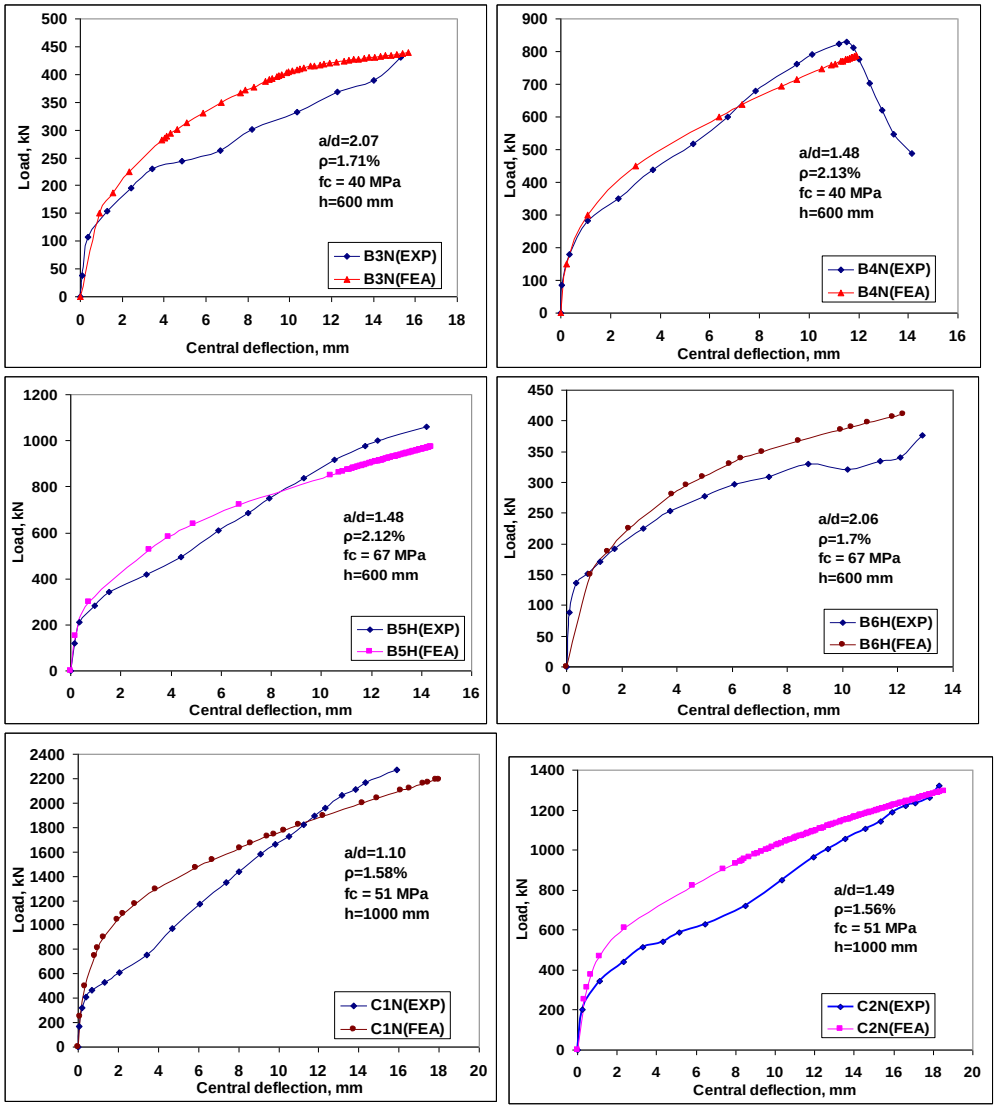

Figure 3 (cont'): FE Versus Experimental Load-Deflection Curves of the Studied Deep Beams

Table 4 : Experimental and predicted ultimate load capacity(Pu),deflection at P_u, diagonal cracking load(Pc), and reserve capacity of GFRP-reinforced concrete deep beams

Specimen	**Experimental**				**Exp/FEA(ABAQUS)**				***Failure Mode****
	Pu, kN	**Δ*u*, *mm***	**Pc, kN**	**Reserve capacity (Pc/ Pu)**	***Pu***	**Δ*u***	Pc	**Reserve capacity**	
A1N	814	12.4	312	0.38	0.97	1.17	0.99	1.02	FC
A2N	471	11.3	187	0.40	1.02	0.93	0.96	0.96	SC
A3N	243	10.9	143	0.59	1.03	0.97	0.92	0.90	SC
A4H	192	9.5	163	0.85	0.93	0.99	1.05	1.13	DT
B1N	1273	9.1	387	0.30	1.04	0.93	0.94	0.89	FC
B2N	799	13.1	287	0.36	1.04	0.95	1.02	0.98	SC
B3N	431	15.3	237	0.55	0.98	0.98	1.05	1.07	SC
B4N	830	11.5	412	0.50	1.05	0.97	1.1	1.05	SC
B5H	1062	14.2	387	0.36	1.09	0.99	0.94	0.85	S
B6H	376	12.9	212	0.56	0.92	1.06	0.94	1.02	DT
C1N	2269	15.9	613	0.27	1.03	0.88	0.99	0.96	SC
C2N	1324	18.3	413	0.31	1.02	0.99	1.01	0.98	S
Mean					1.01	0.98	0.99	0.98	
Standard deviation					0.05	0.07	0.05	0.08	

**DT-diagonal concrete tension failure, FC – flexural compression failure, SC – shear compression failure, S – compression strut failure.*

4.2 Diagonal Cracking Load and Reserve Capacity

Prior to cracking of the concrete, an elastic stress distribution exists in deep members. Cracking disrupts the stress distribution and a major reorientation of the internal forces occurs such that forces tend to flow directly from the loading points to the supports. Arch action involves the formation of compression struts to directly transmit the load to the supports while the flexural reinforcement acts as a tie holding the base of the arch together. Unlike slender members with no web reinforcement, deep members have substantial reserve capacity after diagonal cracking as reported by Wight and MacGregor(2009). The diagonal-cracking strength is defined as the strength at which the first fully developed major diagonal tension crack appears in the shear span(cracking load can be defined in ABAQUS by mointoring the first appearance of crack at a ceratin load increment under the visualization module). The diagonal tension cracking strength was observed to be considerably less than the ultimate strength. Many mechanisms may be responsible for such behavior. However, the major phenomenon is

attributed to the arch action mechanism. Deep RC beams exhibited significantly enhanced shear resistance after first diagonal cracking as a result of strong strut action of concrete in compression. The Pc/Pu(diagonal cracking load/ ultimate load) ratio serves as a measure of the reserve load capacity after the formation of the first inclined crack. The reserve load capacity was analyzed from the experimental observations and F.E results for all beams(Table 4). The ratio Pc/Pu (reserve capacity)in all deep beams lies in the range between 0.27 to 0.85 from experimental results and the same ratio lies in the range between 0.28 to 0.75 as obtained from F.E (Table 4). Andermatt and Lubell (2013B) pointed out in their paper that the low or high reserve load capacity was indicative of the formation of arch action after inclined cracking occurred, this verifies through matching the experimental results with F.E analysis. The mean ratios of experimental-to-predicted (by ABAQUS) of diagonal cracking load is 0.99 at a standard deviation of 0.05, and mean ratios of experimental-to-predicted reserve capacity is 0.98 at a standard deviation of 0.08(Table 4). On the other hand, as reported by Andermatt and Lubell (2013B) in their study that the strut-and-tie model in Canadian code (Canadian Standards Association,2004) gives an average ratio of experimental ultimate capacities to predicted ones equal 0.81, with a standard deviation of 0.16 and the strut-and-tie model in American code (ACI Committee 318, 2008) and Egyptian code (ECP 203-07, 2007) is the same, they give mean of test to predicted values equal 0.60 with standard deviation of 0.2. This confirms that the finite element analysis attained a higher accuracy for predicting of both ultimate load failure and diagonal cracking load than these codes.

4.3 Failure Mechanisms

Table 4 contains four types of failure mechanisms were observed experimentally by Andermatt and Lubell (2013A); these types are:

1. *Diagonal concrete tension failure(DT) or splitting failure*: it occurred in specimens A4H and B6H. The diagonal crack formed in each shear span from the inside edge of the reaction plate toward the inside edge of the loading plate. The diagonal crack extended above the diagonal line between the centerlines of the loading and support plates as shown in Figure 4 .

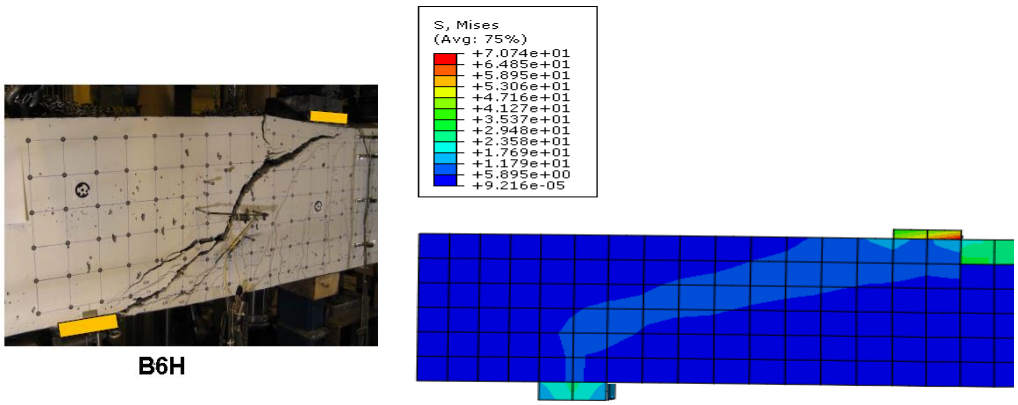

Figure 4: Experimental and Finite Element Pattern of Diagonal Concrete Tension Failure (DT) for Specimen B6H

2. *Flexural compression failure(FC)*: it occurred in specimens A1N and B1N. This type of failure was characterized by the crushing of the concrete in the flexural compression zone between the two loading plates as shown in Figure 5.

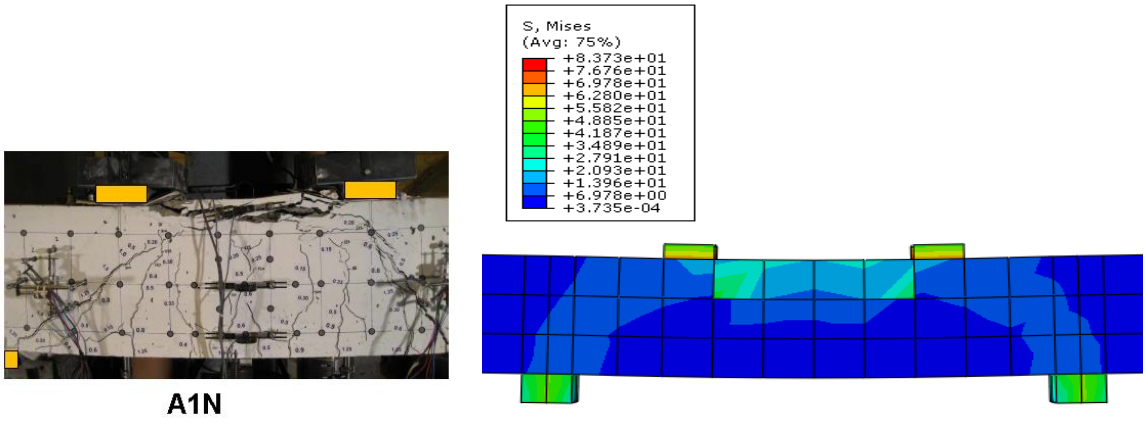

Figure 5: Experimental and Finite Element Pattern of Flexural Compression Failure(FC) for Specimen A1N

3. *Shear compression failure(SC)*: it was the most common failure mode, occurring in six of the specimens(Table 4). Shear compression failure was characterized by the crushing of the concrete in the flexural compression zone at the tip of the main diagonal crack. The main diagonal crack extended from the

inside edge of the support plate towards the inside edge of the loading plate, into the flexural compression zone. In this type of failure, the specimens would fail suddenly with almost no warning and movement would occur along the diagonal crack. Figure 6 shows a typical shear compression failure.

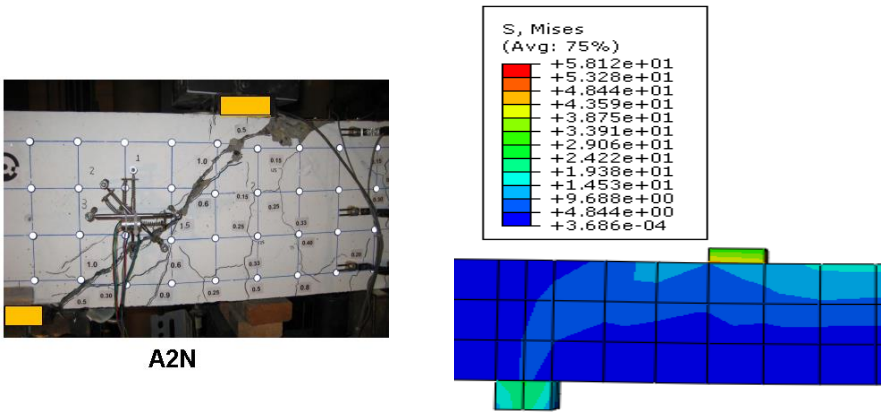

Figure 6 : Experimental and Finite Element Pattern of Shear Compression Failure(SC)for Specimen A2N

4. *Compression strut failure (S):* Failure of the diagonal compression struts occurred in specimens B5H and C2N. In both specimens, one of the diagonal compression struts would fail in a very brittle and noisy manner. Figure7 shows the diagonal compression strut failure in specimen B5H.

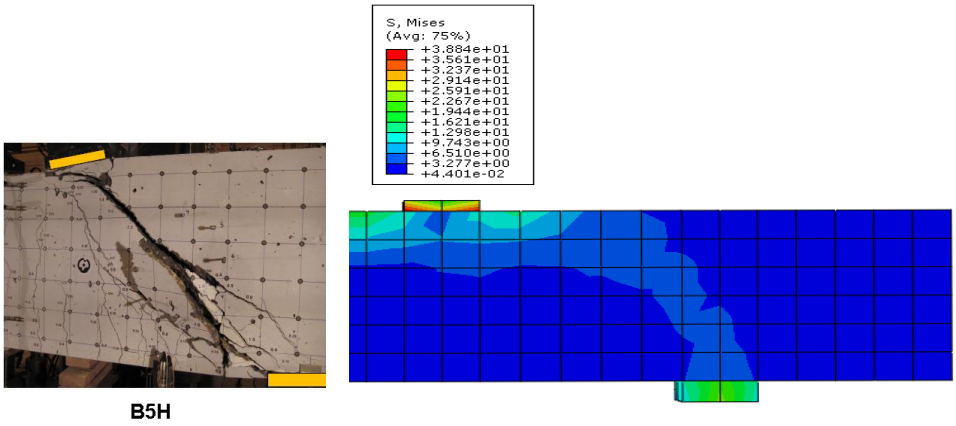

Figure 7: Experimental and Finite Element Pattern of Compression Strut Failure (S)for Specimen B5H

In cases where the specimen failed in shear-compression(SC), the load decreased abruptly upon reaching the ultimate value and failure was brittle. On the other hand, for specimens that failed in flexure(FC), the load remained almost constant with increasing deflection at ultimate, indicating ductile specimen behavior. In all specimens, the cracks propagated towards the loading point as the load was increased. This was accompanied by more flexural-shear cracks along the specimen shear spans. Specimens that did not fail in flexure also experienced diagonal splitting, which eventually led to a shear-compression failure resulting in the crushing of concrete in the compression zone of deep beams. The failure of specimens was sudden and explosive and the most of specimens failed in shear compression as mentioned by Andermatt and Lubell (2013A). ABAQUS can monitor and capture the shape and propagation of cracks during loading till failure. The predictions of the failure modes of all the beams by finite element agree with the experimental observations(Figures 4,5,6 and 7).

4.4 GFRP Bars Reinforcement Strains

Importance of showing tensile reinforcement strains, is it considered as an indicator of whether and to what extent a tied arch mechanism formed in the specimens. In a fully developed tied arch mechanism, the strain level in the reinforcement is expected to be approximately uniform from support to support for both experimental and FE results as shown in Figures 8 ,9 and 10.). Andermatt and Lubell (2013A) reported in their experimental study that for all specimens, the strain distribution between the supports at peak load was approximately constant indicating an arch mechanism had developed. The experimental strain distribution along the bottom layer of GFRP reinforcement of B1N as the load increased is shown in Figure 8 and the anticipated strains by FE is shown in Figure 9, both patterns are typical for all specimens. In the majority of the specimens, the strain in the GFRP at the center of the support was significantly lower than the strain whether read(experimentally) or predicted (by FE) at mid-span. The strain readings of the bottom bar increased rapidly in the vicinity of the first crack, usually in the constant moment region(mid-span). As more cracks formed closer to the supports, the measured strains in the GFRP reinforcement would also increase closer to the support. In the un-cracked regions, strain readings showed minimal strain changes in the GFRP.

As loading progressed, the strains in the reinforcement became similar between the supports indicating the formation of a tied arch mechanism. The strain level in the bottom reinforcement layer outside of the span of specimen B1N is relatively high at the final failure load of 1273 kN. The splitting crack that had formed near the location of the bottom reinforcement was caused by increase in the GFRP reinforcement strain level. The strain of longitudinal reinforcement in all specimens did not reach 60% of ultimate tensile strain of GFRP bars(Table3) throughout the tests. Figure 10 show that the F.E results of generated strain in top layer of GFRP reinforcement which is lower than the generated one in bottom layer, this phenomenon due to that the bottom GFRP

reinforcement anchored a grater amount of force than the upper layers. Consequently, different design codes which incorporated strut and tie method for analysis as Canadian code (Canadian Standards Association, 2004), American code (ACI Committee 318, 2008), and Egyptian code (ECP 203-07, 2007) are not valid for analysis and design of deep beam reinforced with FRP bars, because they are assumed that all layers of reinforcement carry the same tensile stress and so the same strain. However, this is only true when all reinforcement has yielded (as in case of steel bars) , which is not the case with the fully linear elastic as FRP bars.

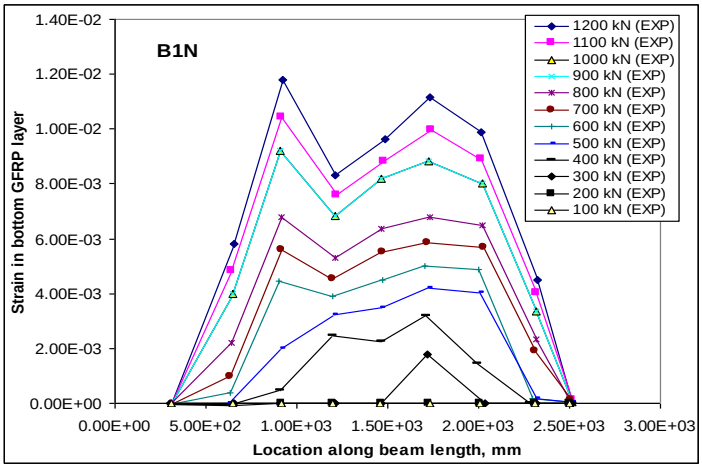

Figure 8 : Experimental Reinforcement Strain Distribution Along the Bottom Layer of Reinforcement as the Load Increased for Beam B1N (Andermatt and Lubell , 2013A)

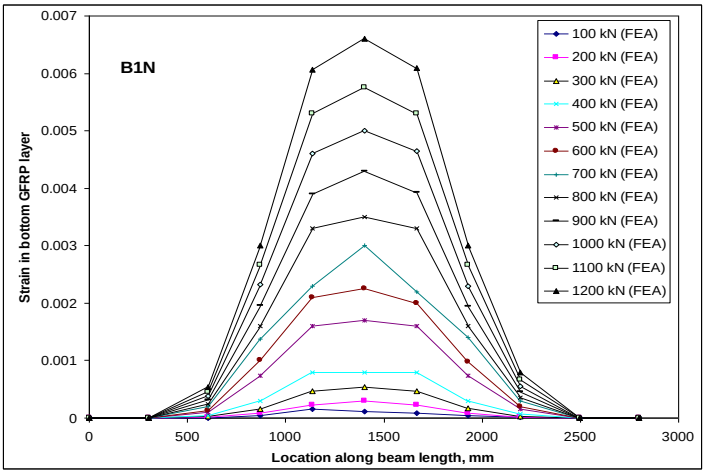

Figure 9 : Predicted Reinforcement Strain Distribution Along the Bottom Layer of Reinforcement as the Load Increased for Beam B1N by ABAQUS

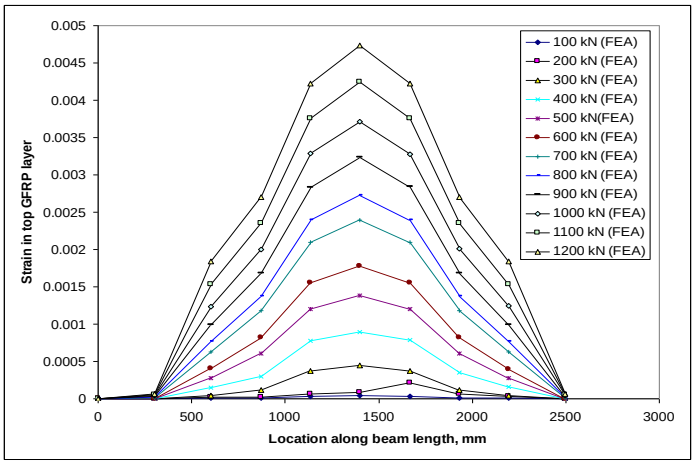

Figure 10 : Predicted Reinforcement Strain Distribution Along the Top Layer of Reinforcement as the Load Increased for Beam B1N by ABAQUS

4.5 *Concrete Strain Distribution*

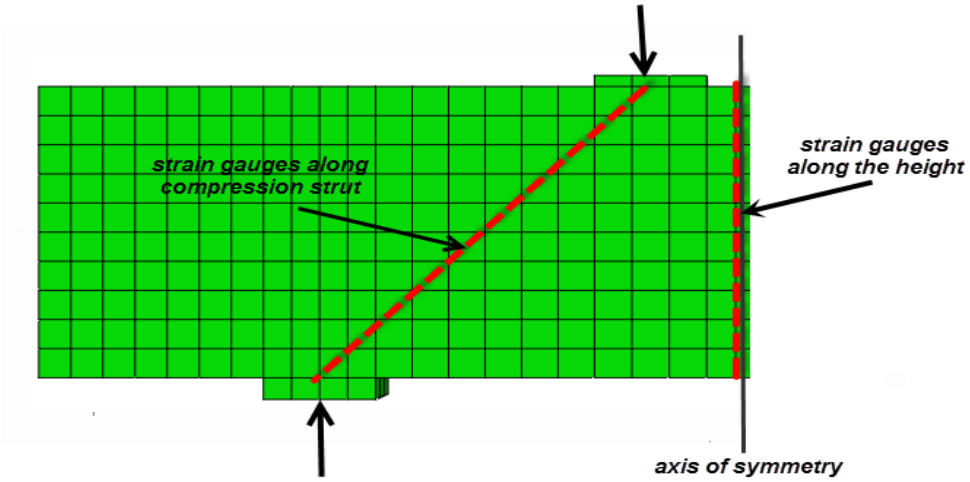

Figure 11: Simulated Locations of Strain Gauges Along the Height of Deep Beam and Compression Strut by Finite Element.

Distribution of strains along the concrete surface of beam height at mid-span and compression strut were modeled by finite element analysis using ABAQUS, the various locations of strain gauges to monitor the strains are shown in Figure 11. Plots of the strain variations determined by the FE analysis along the section height at the mid length and neutral axis depth variations of all beams under first crack load and ultimate load are shown in Figure 12. It shows that the strain distribution in GFRP-reinforced concrete

deep beams is nonlinear. The number of neutral axis (N.A.) at ultimate load is one, while there are more than one neutral axes before ultimate failure. The number of neutral axes decreases with incremental loads and at ultimate stage only one neutral axis is present. The compression strain in the top fiber of the mid-span section increases as the load increases, but in the tension area, the strain predictions were disturbed by the cracks and the flexibility in this area.

As shown in Figure 12, at the ultimate load state, the compressive strain distribution in the concrete is nonlinear as it no longer follows the parabolic shape or intensity linearity of normal(shallow) beams. This condition is due to the predominant effect of the horizontal bar post-cracking, the reduction in the concrete's compression area and the shear deformation that is prevalent in deep beams. Canadian code(Canadian Standards Association, 2004) states that the maximum compression strain for steel-reinforced deep beam design is 0.002, which is lower than for a normal beam(0.003). Till now, it has no provision for FRP-reinforced deep beams. Figure 12 shows that compression strains of most deep beams ranges from 0.001 to 0.002 much lower than those of normal beams reinforced with FRP bars which also equal to 0.003 (ACI Committee 440, 2006) as steel-reinforced shallow beams. This observation should be taken into consideration when designing a deep beam, since the maximum strain at the extreme compression fiber is comparatively small.

The difference in the maximum compression strain in the extreme compression fiber in shallow and deep beams is due to reasons such as the size effect and the load transferring mechanism. The other reason was the concrete strength. In a high strength concrete (HSC) beam section, a shallower compressive stress block is required to equilibrate the tension zone forces. Therefore the neutral axis in a HSC beam is closer to the extreme compression fiber compared to an normal concrete strength (NSC) beam with the same reinforcement ratio. The lower neutral axis depth is expected to result in higher plastic strains in the tension reinforcement, leading to ductile behavior. All these aforementioned reasons justify the fact that GFRP-reinforced deep beams exhibit a lower ultimate strain in the extreme compression fiber. Furthermore, since deep beams have more than one neutral axis before the ultimate load, the section design equation for FRP-reinforced normal(shallow) beams is not valid for deep beams. In addition, it is important to consider the nonlinear behavior of GFRP-reinforced deep beams in the strain and stress distribution. GFRP-reinforced deep beams do not conform to Bernoulli's assumptions for strain and stress distribution. Bernoulli's hypothesis facilitates the flexural design of reinforced concrete structures by allowing a linear strain distribution. Figure 12 shows that GFRP-reinforced deep beams are far from being linearly elastic when the ultimate load is reached. This nonlinearity of strain distribution is due to the shear deformations that are often less obvious in FRP-reinforced shallow beams, but that are significant in GFRP-reinforced deep beams. Thus the internal stresses and behavior of GFRP-reinforced deep beams cannot be determined using ordinary beam theory. This reiterates that deep beams do not conform to the common

hypothesis for shallow beams that plane sections remain planar after bending.The compressive strains along the strut with the highest measured strain around 0.0008. This is lower than suggested by the Canadian code(0.002) (Canadian Standards Association, 2004). As seen in Table 5, the maximum compressive strain has occurred around of mid height of these beams and may not occur in the compression strut trajectory line. This has an important implication in the design of GFRP-reinforced deep beams, particularly when using the Canadian code.

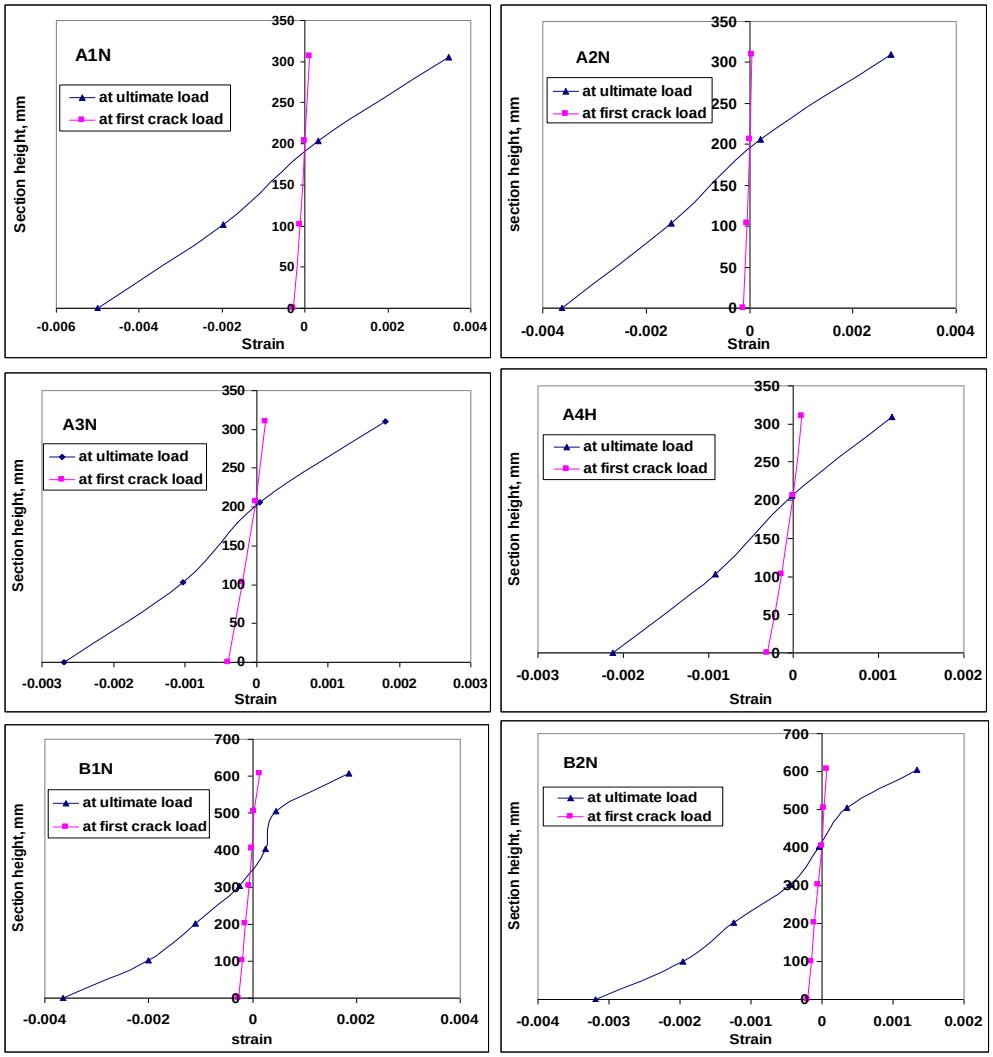

Figure 12: Concrete Strain Distributions and Neutral Axis Depth Variations Along the Section Height at Mid-Span of all Studied GFRP-Reinforced Deep Beams under First Crack Load and Ultimate Load using FE Modeling.

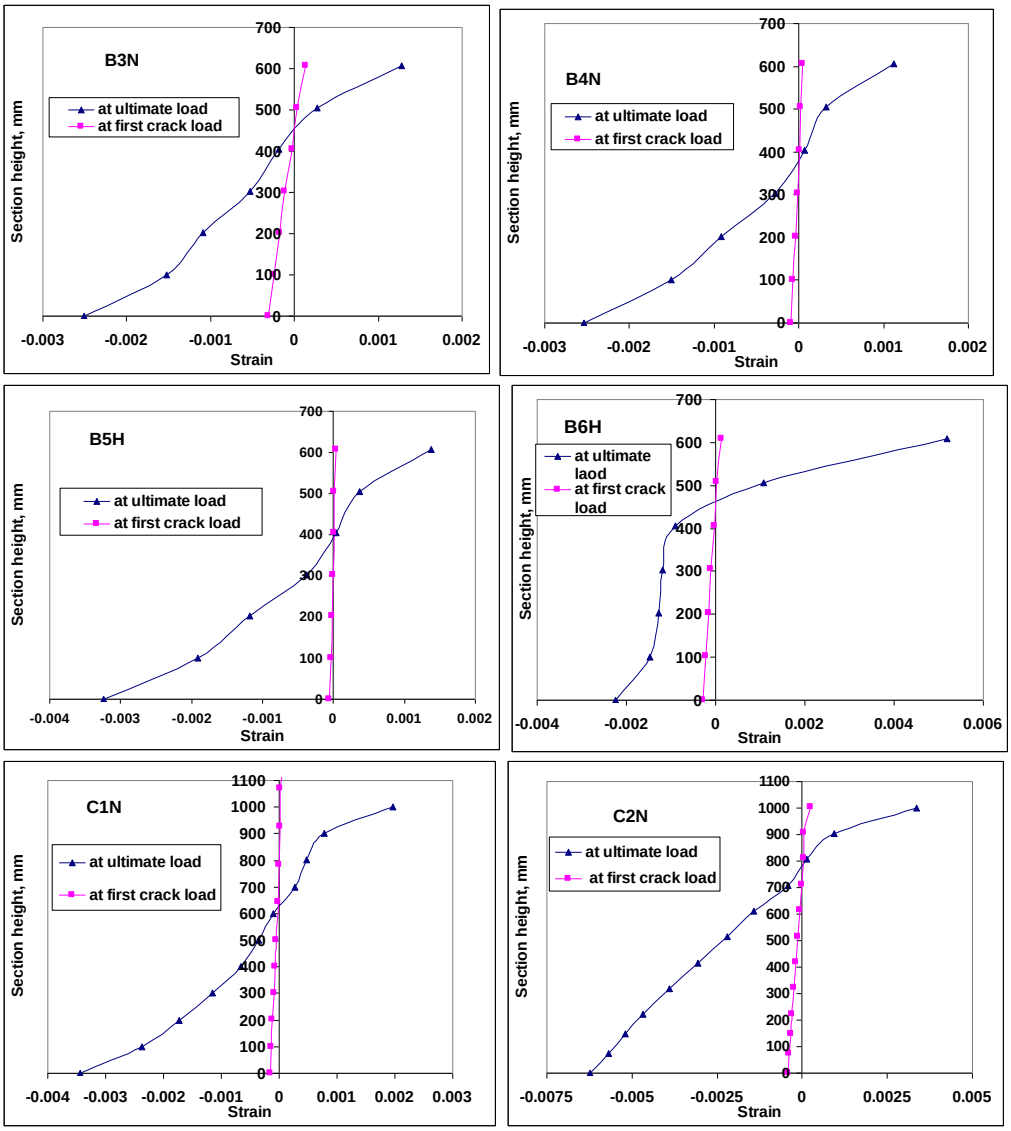

Figure 12 (cont'): Concrete Strain Distributions and Neutral Axis Depth Variations Along the Section Height at Mid-Span of all Studied GFRP-Reinforced Deep Beams under First Crack Load and Ultimate Load using FE Modeling (Continued).

Table 5 : Maximum compressive strain along mid-span locations and compression strut line

Specimen	ε_{cu} at mid -span	ε_{cu} along the strut line
A1N	0.00346	0.000713
A2N	0.00273	0.000794
A3N	0.00180	0.000642
A4H	0.00115	0.000546
B1N	0.00185	0.000574
B2N	0.00133	0.000606
B3N	0.001275	0.000532
B4N	0.00111	0.000632
B5H	0.00138	0.000591
B6H	0.005195	0.000509
C1N	0.00197	0.000669
C2N	0.00335	0.000645

ε_{cu}: concrete compressive strain at ultimate load

4.6 Influence of FRP Bar Type on Behavior of Deep Beam

This section discusses the difference between behavior of GFRP-reinforced deep beam and CFRP-reinforced deep beam. To achieve this purpose, FE models were constructed by ABAQUS for some selected specimens as A2N, A4H, B1N, B6H, and C1N with replacing GFRP bars by CFRP bars which were modeled as elastic isotropic one dimensional material until failure as recommended by Al-Musallam *et al*. (2103), with a common properties (E_f*= 120,000MPa*, f_{fu} *= 1600 MPa, and* υ *= 0.2*) as specified by Farghaly and Benmokrane (2013). Figure 13 shows the comparison between results, it can be seen that deep beams reinforced with GFRP bars exhibit a significant reduction in stiffness after the initiation of the first crack in comparison with the same beam reinforced with CFRP reinforcement. At the ultimate load, the mid-span deflection of GFRP-reinforced deep beams as A2N, A4H, B1N, B6H, and C1N was about 3.5, 2.5, 2.4, 3.6, and 1.7 times more than the CFRP-reinforced ones respectively. This behavior is attributed to the low elastic modulus of the GFRP bars(~40,000MPa) compared to that of the CFRP bars(120,000 MPa). The low modulus of elasticity of the GFRP bars affects the ability of these bars to control concrete cracking. This decreases the tension stiffening effect for concrete between cracks leading to a reduced effective moment of inertia and hence large deflections, as was experimentally confirmed by Farghaly and Benmokrane (2013).

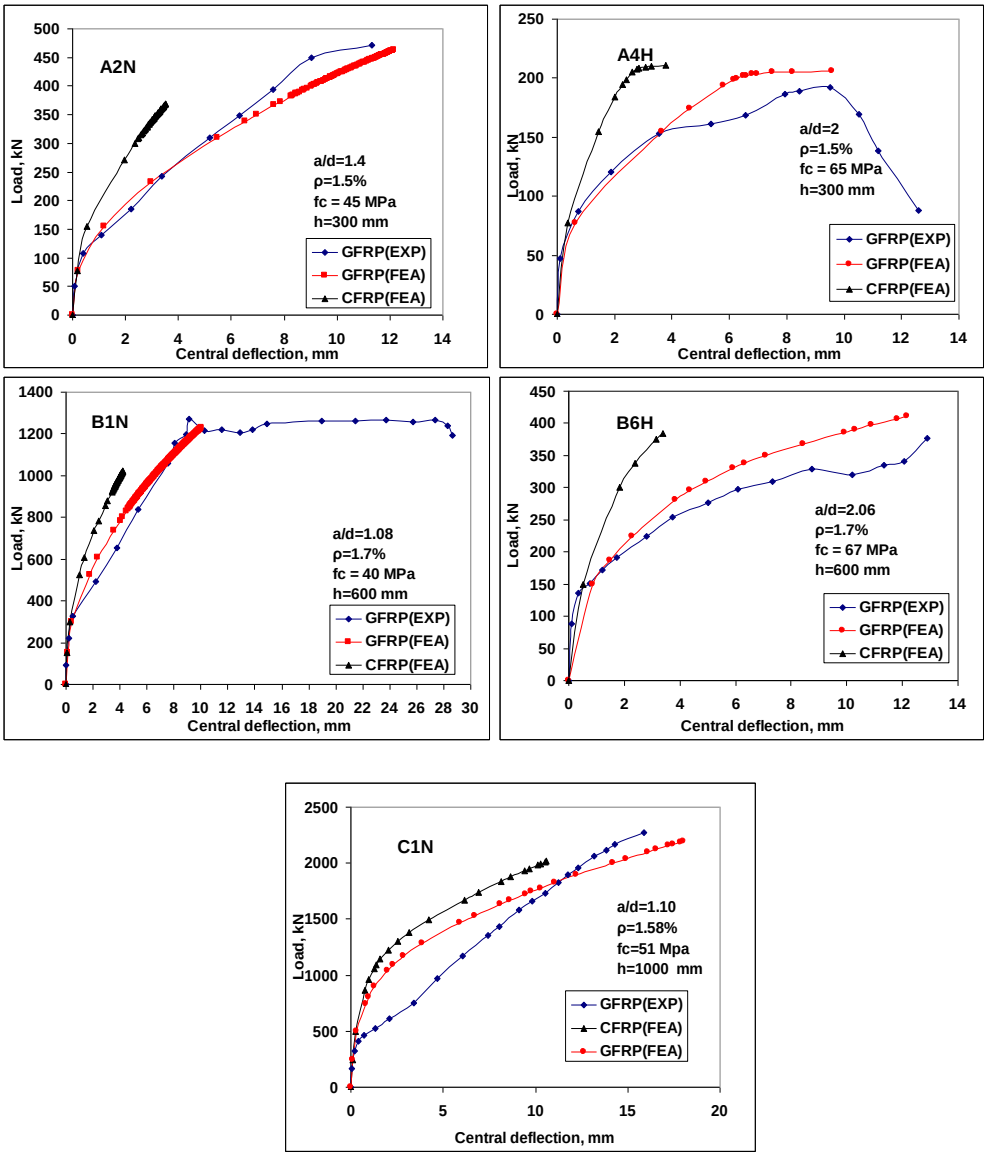

Figure 13: Effect of FRP bar type on load-deflection response of deep beams

5.0 Conclusions

In this paper, the nonlinear finite element analysis by ABAQUS was used to predict the behavior and strength of concrete deep beams reinforced with GFRP bars in large scale. The agreement between the numerical simulations and experimental findings demonstrate the overall accuracy and reliability of the analytical models in predicting the response of that this new type of structural elements. Based on the results of the numerical simulations and comparisons with experimental data, the following conclusions were reached:

1. The results from the finite element simulation agree very well with the experimental observations, especially with regards to load-deflection response, crack patterns at different load stages, failure modes and mechanisms, GFRP bars strains and concrete strains. All these indicate that the constitutive models used for concrete and GFRP bars by ABAQUS able to capture the fracture behavior of GFRP-reinforced deep beam accurately. Consequently, this method may be used for the nonlinear analysis and design of such elements very efficiently.

2. In general, the experiment results of GFRP-reinforced concrete deep beams and the FEM analysis by ABAQUS were in very good agreement, The mean ratios of experimental-to-predicted values for : ultimate load capacities equal 1.01 with standard deviation of 0.05, mid-span deflection at ultimate load equal 0.98 with standard deviation of 0.07, diagonal cracking load equal 0.99 with standard deviation of 0.05, and reserve capacity equal 0.98 with standard deviation of 0.08.

3. The present finite element study which has been verified through the experimental results demonstrated, that the abundant reserve capacity was available after the formation of the main diagonal cracks, indicated the GFRP-reinforced concrete deep beams were able to redistribute the internal forces and develop an arch mechanism.

4. ABAQUS can monitor and capture the shape and propagation of cracks during loading till failure. The predictions of the failure modes of all the beams by finite element agree well with the experimental observations.

5. Finite element analysis and experimental results shows, as loading progressed, the strain distribution in the longitudinal GFRP reinforcement became approximately uniform between the supports indicating the formation of a tied arch mechanism.

6. FE analysis in this research shows that the dependence on the current design codes as ACI 318-08, CSA A 23.3-04 and ECP-203-07 in analysis and design of FRP-reinforced concrete deep beams is not accurate because they are assumed that all layers of reinforcement carry the same tensile stress and so the same strain, this in not true in case of FRP reinforcement. However, this is only true when all reinforcement has yielded (as in case of steel bars) , which is not the case with the fully linear elastic as FRP bars.

7. Concrete strain distribution in GFRP-reinforced concrete deep beams is nonlinear, they do not conform to Bernoulli's assumptions for strain and stress distribution. This nonlinearity of strain distribution is due to the shear deformations that are often less obvious in FRP-reinforced shallow beams, but that are significant in GFRP-reinforced deep beams.

8. The number of neutral axis at ultimate load is one, while there are more than one neutral axes before ultimate failure. The number of neutral axis decreases with incremental loads and at ultimate load stage only one neutral axis is present.

9. Maximum compression strain in the extreme compression fiber of most GFRP-reinforced deep beams at ultimate stage of loading ranges from 0.001 to 0.002 much lower than those of shallow beams reinforced with FRP bars (0.003). This observation should be taken into consideration when designing a deep beam, since the maximum strain at the extreme compression fiber is comparatively small.

10. The strains measured along the compression strut were less than the value of 0.002 proposed by the Canadian code, with the highest measured strain reaching about 0.0008. This study shows that the maximum compression strain may not occur in the compression strut trajectory line, the maximum compressive strain has occurred around of mid height of GFRP-reinforced deep beams. This has an important implication in the design of those beams, particularly when using the Canadian code.

11. Since, the nonlinear strain distribution dominates the GFRP-reinforced deep members behavior. Accordingly, finite element analysis is most appropriate technique for analysis and design of such beams.

12. Deep beam reinforced with GFRP bars showed different behavior than that of beam reinforced with CFRP bars due to the low elastic modulus of GFRP bars. At ultimate load level, the deflection of the GFRP-reinforced deep concrete beam was in the range of 2 to 4 times more than the CFRP- reinforced deep beam resulting from the low elastic modulus of the GFRP bars. Thus, the

deflection, instead of strength will govern the design for concrete deep beam reinforced with FRP bars.

13. Future research work must be included the formulation of a constitutive model for time dependent effects such as concrete creep, shrinkage and fire exposure. Also, experimental testing and finite element analysis of continuous deep beams reinforced with FRP bars must be investigated.

References

ABAQUS (2014): Standard Version 6.13-4. The ABAQUS Software is a product of Dassault Systèmes Simulia Corp. Hibbitt Karlsson & Sorensen Inc.USA.

ACI Committee 318(2008): Building Code Requirements For Structural Concrete and Commentary. (ACI 318-08). American Concrete Institute. Farmington Hills. Michigan. United States.

ACI Committee 440(2006): Guide for the Design and Construction of Structural Concrete Reinforced with FRP Bars (ACI 440.1R-06). American Concrete Institute. Farmington Hills. Michigan. United States.

Al-Musallam, T.; El-Sanadedy, H.; Al-Salloum, Y.; and Al-Sayed, S.(2013): Experimental and Numerical Investigation for the Flexural Strengthening of RC Beams Using Near-Surface Mounted Steel or GFRP Bars. Constr. and Build. Mat. J. 40, 145-161.

Andermatt, M. and Lubell, A. (2013A): Behavior of Concrete Deep Beams Reinforced with Internal Fiber-Reinforced Polymer—Experimental Study. ACI Str. J. 110, 585-594.

Andermatt, M. and Lubell, A.(2013B): Strength Modeling of Concrete Deep Beams Reinforced with Internal Fiber-Reinforced Polymer . ACI Str. J. 110, 595-605.

Canadian Standards Association(2004): Design of concrete structures(A23.3-04). Canadian Standards Association. Mississauga. Ontario. Canada.

ECP 203-07(2007): Egyptian Code for Design and Construction of Concrete Structures. Housing & Building National Research Centre.

Enem, J.I., Ezeh, J.C., Mbagiorgu, M.S.W., and Onwuka, D.O(2012): Analysis of deep beam using Finite Element Method. Int. J. of Ap. Sc. and Eng. Res. 1, 348-356.

Farghaly, A., and Benmokrane, B.(2013): Shear Behavior of FRP-Reinforced Concrete Deep Beams without Web Reinforcement. J. of Com. for Const.. 17, 1-10.

Islam, S. and Khennane, A.(2012): Experimental Verification of Automated Design of Reinforced Concrete Deep Beams. SIMULIA Customer Conference,1-15.

Malm, R(2009):. Predicting shear type crack initiation and growth in concrete with non-linear finite element method. PhD thesis Department of Civil and Architectural ngineering. Royal Institute of Technology (KTH). Stockholm.

Nawy, E. G. (2003): Reinforced concrete: A fundamental approach, Prentice Hall, Upper Saddle River, NJ.

Wight, J. K. and MacGregor, J. G. (2009): *Reinforced Concrete: Mechanics and Design (5th edition)*, Pearson Prentice Hall, Upper Saddle River, New Jersey.